A decentralized water/electricity cogeneration system integrating concentrated photovoltaic/thermal collectors and vacuum multi-effect membrane distillation

Qian Chen[1,*], Muhammad Burhan[1], Faheem Hassan Akhtar[1], Doskhan Ybyraiymkul[1], Muhammad Wakil Shahzad[1,2], Yong Li[3], Kim Choon Ng[1,*]

1. *Water Desalination and Reuse Center, King Abdullah University of Science and Technology, Thuwal 23955, Saudi Arabia*
2. *Northumbria University, Newcastle upon Tyne, United Kingdom*
3. *College of Environmental Science and Engineering, Donghua University, Shanghai 201620, China*

*Corresponding Authors, email: chen_qian@u.nus.edu; kimchoon.ng@kaust.edu.sa

Abstract: Cogeneration of electricity and freshwater by integrating photovoltaic/thermal collectors and desalination systems is one of the most promising methods to tackle the challenges of water and energy shortage in remote areas. This study investigates a decentralized water/electricity cogeneration system combining concentrated photovoltaic/thermal collectors and a vacuum multi-effect membrane distillation system. The merits of such a configuration include high compactness and improved thermodynamic efficiency. To evaluate the long-term production potential of the proposed system, a thermodynamic analysis is firstly conducted. Under the climatic conditions of Makkah, Saudi Arabia, the system can convert ~70% of the solar irradiance into useful energy. The annual productivity of electricity and distilled water are 562 kWh and 5.25 m^3, respectively, per m^2 of the solar collector area. Electricity and water production rates are found to be impacted by hot water flowrate, feed seawater flowrate and heat storage tank dimension, while the overall exergy efficiency stabilizes at 25-27%. Based on the production rates, an economic analysis is conducted through life-cycle cost analysis. The final desalination cost is calculated to be \$0.7-4.3/m^3, depending on the solar collector cost and the electricity price. The derived results will enable a more in-depth understanding of the proposed solar-driven water/electricity cogeneration system.

Keywords: concentrated photovoltaic/thermal collector; vacuum multi-effect membrane distillation; water/electricity cogeneration; decentralized;

1. Introduction

Energy and water are two resources that are indispensable for the continuation of human society, while the supply of primary energy and freshwater is not enough to meet the global demand. Currently, nearly 1.2 billion people have no access to electricity, and 800 million people cannot get enough potable water [1]. The deficit is expected to increase due to the growth of the global population, which will lead to 50% and 100% increase in water and energy demand, respectively, in 2050 [2]. On the other hand, the primary sources of energy and water on the earth are degrading and depleting at an alarming rate [3], making the situation more critical. Although desalination offers a sustainable solution to the growing water deficit, most of the desalination processes are energy-intensive, and they will place more burdens on the existing energy supply. Therefore, it is of great impetus to explore renewable energy sources for desalination and power generation in order to tackle the challenges associated with water and energy shortages [4, 5].

Solar energy is the most promising type of renewable energy sources. It can be converted into heat or electricity, and the collected heat can be further used to generate electricity [6, 7] or drive other thermal systems. Solar energy is also an ideal energy source for desalination due to high solar radiance in the water-

scarce regions. Most of the existing desalination technologies, e.g., multi-effect distillation (MED), reverse osmosis (RO), and membrane distillation (MD), can be driven by electricity or heat generated by solar collectors. Askari and Ameri [8] proposed a water/electricity cogeneration system integrating a concentrated solar power (CSP) plant and a MED plant. The levelized cost of water was estimated to be 1.63-3.09 $/m^3. Li et al. [9] proposed a hybrid CSP-RO plant. The optimum thermal efficiency was found to be 18-20%. Soomro and Kim [10] evaluated a cogeneration system combining a CSP plant and a direct contact membrane distillation unit. The levelized costs for electricity and water were calculated to be $0.13/kWh and $0.392/m^3, respectively. Iaquaniello et al. [11] presented a hybrid CSP-RO-MED system. The system enabled flexible production of power and water, and the cost for water was found to be €1/m^3.

Comparing with CSP plants, photovoltaic (PV) collectors can convert sunlight into electricity directly. Also, they are cheaper and enable small-scale applications such as rooftop installation. For desalination purposes, integrated photovoltaic/thermal (PV/T) collectors can be employed to simultaneously produce electricity and heat. Several desalination systems driven by PV/T collectors have been reported. Eltawil and Omara [12] proposed a single-slope solar still enhanced by a PV/T collector, a water spray, and a solar air collector. Such an integrated design enhanced the water yield by 51-148% compared with a conventional solar still. Yari et al. [13] integrated a solar still with a semitransparent photovoltaic module placed on evacuated tube collectors. The daily freshwater yield was reported to be 4.77 kg/m^2, while the electricity generation rate was 483.2 Wh/m^2. Pouraj et al. [14] used both the generated heat and electricity generated by the PV/T collector to drive a solar still. Such a configuration increased the freshwater productivity by three times, and the PV efficiency was improved by 38%. Gabrielli et al. [15] analyzed a humidification-dehumidification (HDH) desalination system coupled with PV/T collectors. A higher feed flowrate increased freshwater productivity but reduced electricity output. Anand and Srinivas [16] conducted a parametric analysis on a PV/T-HDH desalination system, and the highest PV efficiency was observed to be 16.6%. Giwa et al. [17] evaluated an air-heated HDH system driven by waste heat recovered from an air-cooled PV system. Under the climatic condition of Abu Dhabi, UAE, the recovered heat was able to produce 2.28 L/day freshwater per m^2 of collector area.

A major disadvantage of the solar stills and HDH cycles is the low productivity, which is attributed to the limited vapor carrying capability of air [18]. Additionally, the existence of air leads to poor heat and mass transfer, making the system bulky. These limitations can be overcome by using more advanced desalination technologies, such as vacuum membrane distillation (VMD). A VMD module operates under vacuum conditions with no air inside the system. Therefore, heat and mass transfer are promoted, leading to higher productivity. Also, the implementation of the membrane as the separation interface reduces the required space for vapor, making the system more compact. Among the various VMD configurations, the vacuum multi-effect membrane distillation (V-MEMD) system demonstrates high production rates and low specific energy consumption due to effective internal heat recovery [19, 20]. The gained-output-ratio (GOR) is reported to be 2-3 for a module with four effects [19]. Moreover, it is able to achieve a recovery ratio of more than 40%, which is one order of magnitude higher than other membrane distillation systems [21].

In light of these promising features, V-MEMD is a perfect candidate for integration with PV/T collectors for standalone operation. However, there is a lack of literature investigating the combination of integrated PV/T and V-MEMD. Chafidz et al. [22] and Andrés-Mañas et al. [23] proposed solar desalination systems based on V-MEMD, but both studies employed solar thermal collectors instead of an integrated PV/T module. The reason is that the hot water temperature provided by an integrated PV/T collector is too low (usually below 45 °C) for V-MEMD operation. To provide higher hot water temperatures for V-MEMD, a concentrated photovoltaic/thermal (CPV/T) module should be employed [24, 25]. Ong et al. [26] proposed the concept of integrating V-MEMD with CPV/T. The system is expected to be able to convert >80% of solar irradiation into useful energy. However, their study only analyzed the V-MEMD module, while the

CPV/T module was not covered. Besides this paper, no other study is available on a water/electricity cogeneration system combining V-MEMD and CPV/T. Several critical questions on this system remain to be explored and clarified. Firstly, the system's annual productivity under different climatic conditions is crucial to access its true potential, yet such information is not available. Secondly, the CPV/T and V-MEMD modules impact each other when integrated, which requires design and operation strategies that are different from the standalone systems. However, a parametric study on the design and operational variables has not been conducted for the integrated system. Thirdly, since the system has two different outputs, i.e., electricity and freshwater, an exergy analysis will provide deeper thermodynamic insights that cannot be obtained from energy analysis, but such an analysis has not been performed. Finally, the economic viability of the integrated system remains to be evaluated.

In this work, we investigate a decentralized water/electricity cogeneration system integrating CPV/T and V-MEMD. A compact CPV/T design is employed for solar energy harvesting and conversion. The generated electricity is supplied to the users, while the collected heat is stored in a hot water tank and utilized to drive a V-MEMD module. A mathematical model will be developed for the proposed system based on previous knowledge and understandings of the subsystems. By employing the developed model, the long-term productivity of water and electricity will be estimated under the climatic conditions of several cities to provide a reliable and robust basis for future design. The impacts of different design and operation parameters on productivity and exergy efficiency are also to be evaluated. Finally, the cost of water will be estimated under various market conditions to assess the economic viability of the proposed system. The novelty and originality of this study is summarized as follows: (1) a compact water/electricity cogeneration system enabling rooftop installation is proposed; (2) a mathematical model is to be developed and validated to enable design and performance evaluation of the proposed system; (3) in-depth thermodynamic and thermoeconomic analyses will be presented for better understanding of the system performance.

2. System description

The proposed water/electricity cogeneration system consists of a series of concentrated photovoltaic/thermal (CPV/T) collectors, a hot water tank, a vacuum multi-effect membrane distillation (V-MEMD) module, a feed tank, and a distillate tank. Figure 1 shows the simplified system layout. The CPV/T collectors convert solar irradiance into both electricity and heat. The generated electricity is supplied to the users, and water is circulated through the cells to carry the generated heat to the hot water tank, which powers the V-MEMD system. In the V-MEMD module, hot water heats the seawater supplied from the seawater feed tank. The seawater then partially evaporates, and the produced vapor is directed to the following effect to be condensed. In the next effect, the condensation heat is reused to heat the seawater and further induce evaporation. The process is repeated several times in the subsequent effects, and vapor produced in the last effect is condensed in an external condenser.

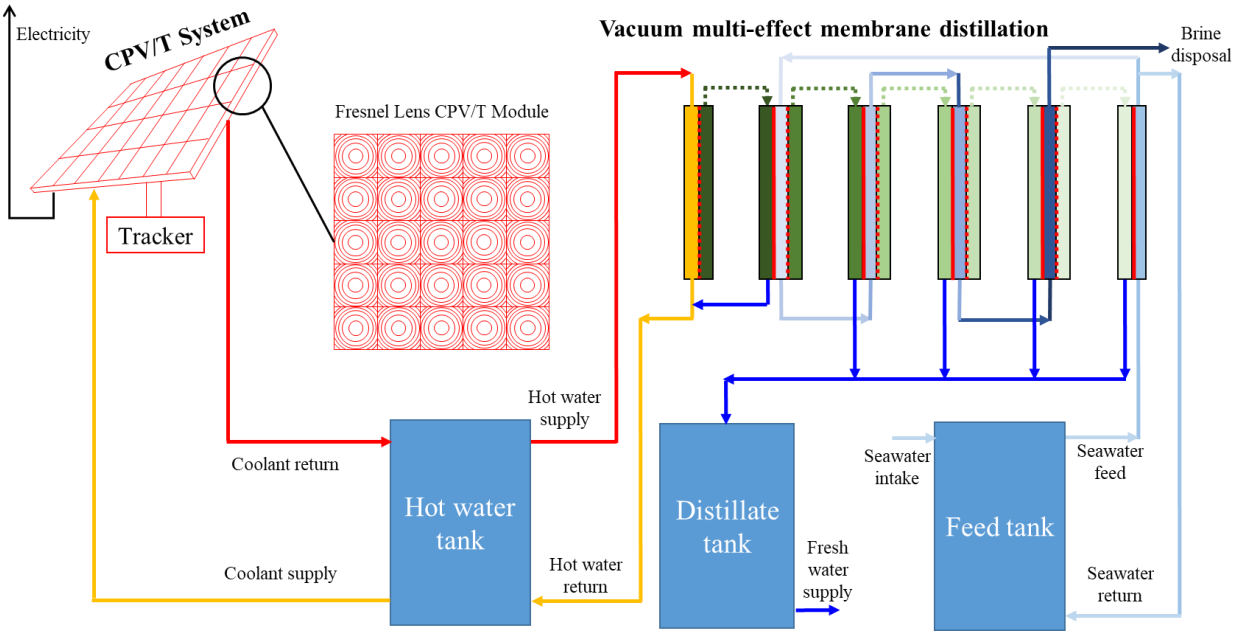

Figure 1. Schematic diagram of the proposed solar-driven electricity/water cogeneration system

Figure 2(a) shows the working principle of a CPV/T module, consisting of Fresnel lenses, glass homogenizers, solar cells, heat sink, and a two-axis solar tracker. Solar radiation is concentrated by the Fresnel lenses, and glass homogenizers are placed at the focal points of the lenses to distribute the rays onto the solar cells uniformly. The solar cells convert a portion of the solar radiation into electricity, while the remaining radiation is dissipated as heat. Coolant is circulated below the cells to absorb the generated heat, which not only lowers the cell temperature and improves the cell efficiency but also recovers the heat for desalination application. The function of the two-axis solar tracker is to trace the direction of the sunlight.

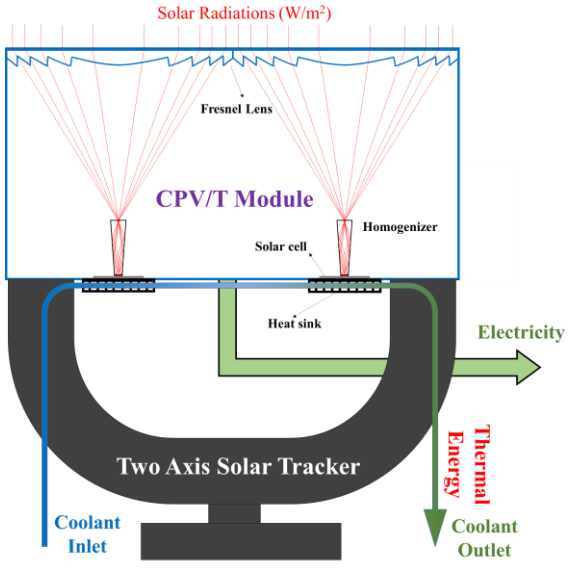

(a)

(b)

Figure 2. Concentrated photovoltaic/thermal system; (a) schematic diagram and (b) pictorial view

To enable rooftop installation, the mini-dish CPV/T modules developed in our previous studies [27, 28] are implemented, as shown in Figure 2(b). Each module consists of four multi-junction cells (MJC) and a 2 × 2 array of Fresnel Lenses. Triple-junction (InGaP/InGaAs/Ge) solar cells, provided by the Arima Photovoltaic and Optical Corporation, are employed in this study. The Fresnel lens array is made of PMMA plastic and has a dimension of 120 mm × 120 mm, while the dimension of each MJC is 5.5 mm x 5.5 mm. The homogenizer is made of quartz material, and its inlet aperture is 23 mm × 23 mm. The whole CPV/T module is mounted on a two-axis solar tracker to track beam radiation with an accuracy of 0.1º.

The V-MEMD system has a similar process flow with the multi-effect distillation (MED) system, and membranes are employed at the evaporation interface to separate water and vapor. The merits of V-MEMD include lower energy consumption, high compactness and high recovery ratio. A V-MEMD module consists of a steam raiser, several production effects, and a condenser, as shown in Figure 3(a). During operation, hot water circulates through the steam raiser and partially evaporates. The produced vapor diffuses across the membrane and is directed to the first effect, where it condenses on the surface of the condensation foils. The condensation heat is absorbed by the feed seawater flowing through the other side of the foils. The seawater starts to evaporate after reaching the saturation temperature that corresponds to the pressure in the first effect. The produced vapor crosses the membrane and flows to the condensation surface in the second effect. Concurrently, the seawater leaving the first effect is directed to the feed channels of the second effect. The pressure in the second effect is lower so that a repetitive process of vapor condensation-seawater evaporation is allowed to happen. The following effects are subjected to successively lowered pressure conditions so that the aforementioned processes can be further repeated. Finally, the vapor produced in the last effect is condensed in an external condenser. Seawater is employed as the cooling media in the condenser to recover the condensation heat. Afterward, a portion of the seawater is supplied to the first effect, while the rest returns to the feed tank. The distillate of the first effect is mixed with the hot water and returned to the heat storage tank, while the remaining distillate flows to the distillate tank.

(a)

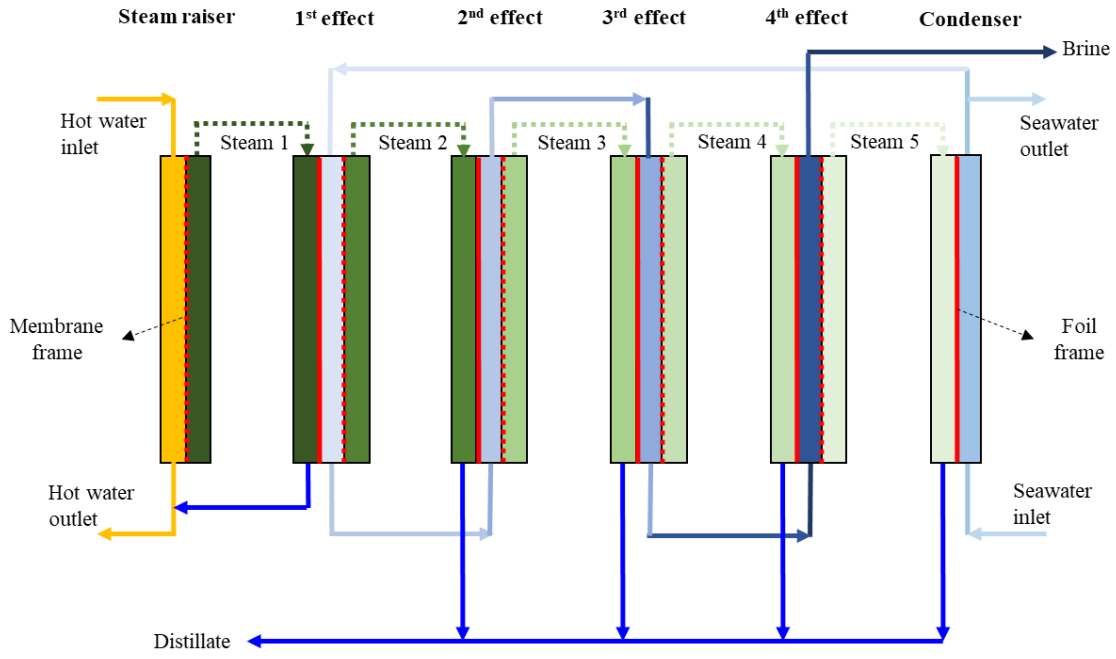

(b)

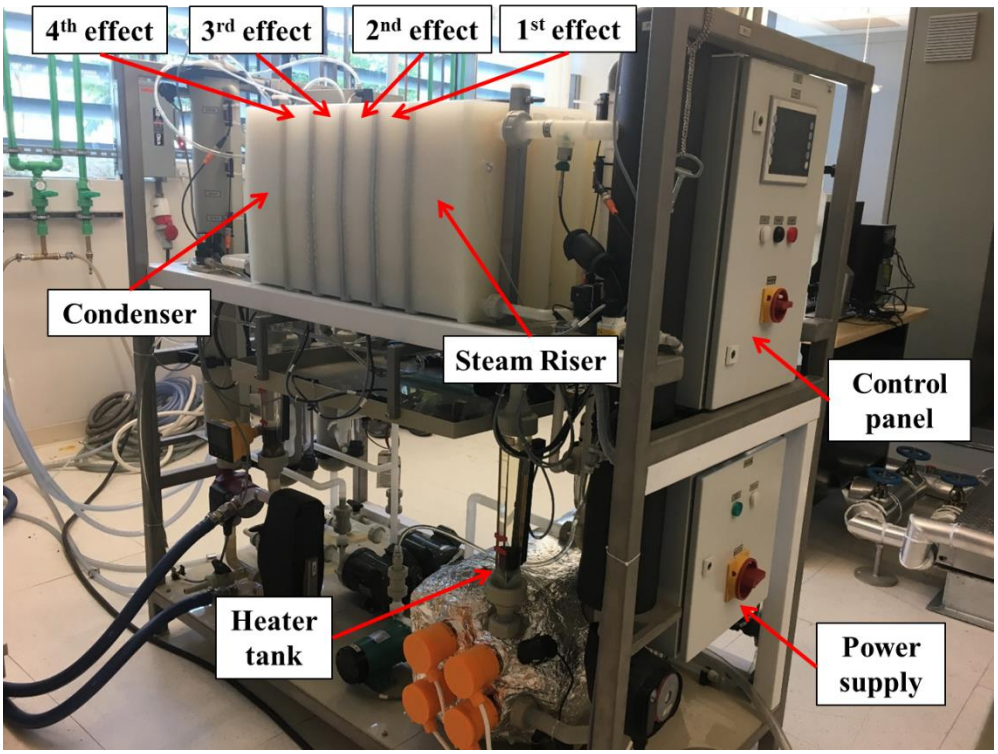

Figure 3. (a) Schematic diagram of the vacuum multi-effect membrane distillation system; (b) pictorial view of a four-effect V-MEMD module

The V-MEMD module developed by MEMSYS is selected in the current study for desalination purposes. A pictorial view of the module is shown in Figure 3(b). It is made up of flat-sheet membrane frames and condensation frames. Polytetrafluoroethylene (PTFE) membranes with a pore size of ~0.2 μm and a thickness of 0.12-0.2 mm are used to make the membrane frames, and the condensation frames are made of polypropylene (PP) foils. Each membrane frame includes two PTFE membranes, and one condensation frame has two PP foils. Holes are opened at the corners of the frames for different streams (seawater and vapor) to enter and exit. Both membrane and foil frames have a dimension of 0.33 m × 0.48 m. In a standard V-MEMD module, the steam raiser consists of 17 membrane frames, and the condenser consists of 17 foil frames. Therefore, both of them have a heat/mass transfer area of 5.38 m^2. These frames are separated by filament spacers, which are specially designed for optimal flow distribution. The production effects are made up of alternating membrane frames and foil frames, with each effect having 5 membrane frames (total membrane area 1.58 m^2) and 6 foil frames. More details on the module design can be found in our previous publications [18, 20].

3. Mathematical modelling

The thermodynamic and economic performances of the proposed system will be evaluated via mathematical simulations. A process model is firstly developed to predict the productivity and thermodynamic efficiencies of the system. Afterward, the economic performance will be derived based on production rates of electricity and freshwater and the costs of different components.

3.1 Thermodynamic modelling

The thermodynamic model covers the governing equations for the solar collector, the hot water tank, and the desalination module. These equations are derived from heat and mass balances in these components as well as heat and mass transfer analysis. Several performance indicators will be introduced to quantify the efficiency of the system.

CPV/T module. The CPV/T system is analyzed by considering the conversion efficiency of the solar cells as well as various energy losses, including optical losses, inverter losses, and heat losses. Solar radiation reaching the cells is calculated as

$$G_{cell} = DNI \times \eta_{opt} \times \frac{A_{lens}}{A_{cell}} \quad (1)$$

where *DNI* is the direct normal irradiance and η_{opt} is the overall optical efficiency of the Fresnel lens and the homogenizer. A_{lens} and A_{cell} are the areas of the lens and the cells, respectively.

A portion of the incoming rays is converted to electricity by the solar cells, while the rest is dissipated as heat. They are expressed as

$$\dot{E} = G_{cell} \times A_{cell} \times \eta_{cell} \times \eta_{inv} \quad (2)$$

$$\dot{Q} = G_{cell} \times A_{cell} \times (1 - \eta_{cell)} \times (1 - \eta_{loss}) \quad (3)$$

In the above equations, η_{cell} and η_{inv} are the cell efficiency and inverter efficiency, respectively, while η_{loss} is the heat loss to the ambient.

The generated heat is recovered by the circulating fluid, and the process is modelled as

$$\dot{Q} = \dot{m}_{sl} c_{p,sl} \times (T_{sl,out} - T_{sl,in}) \quad (4)$$

where $\dot{m}_{sl}$ is the flowrate of the circulating fluid, $c_{p,sl}$ is the specific heat, and $T_{sl,in}$ and $T_{sl,out}$ are the fluid temperature when entering and leaving the solar cells, respectively.

The key parameter that defines the performance of the CPV/T module is the cell efficiency, η_{cell}. It is derived using the simple diode model. Based on the model theory, the power output of single MJC is calculated as [29]

$$\dot{P} = IV = V\{I_0 \left[\exp\left(\frac{qV}{nkT_{cell}}\right) - 1\right] - I_{SC}\} \quad (5)$$

where *I* and *V* are the current and voltage, respectively. *q* is the electrical charge, *k* is the Boltzman's constant, and *n* is the diode ideality factor. I_o is the diode saturation current, and I_{SC} is the short circuit current.

In order to find out I_o, the open circuit voltage condition is invoked, i.e., the current is zero and voltage equals to V_{OC}, the open circuit voltage. Therefore, I_o is derived as [27]

$$I_0 = \frac{I_{SC}}{\exp\left(\frac{qV_{OC}}{nkT_{cell}}\right) - 1} \quad (6)$$

The open circuit voltage and the short circuit current of MJC can be calculated through the cell performance variation against concentration at temperature T_0 [27]

$$V_{OC}(T_{cell}, G_{cell}) = V_{OC}(T_0, G_{cell}) + (T_{cell} - T_0) \times \frac{dV_{OC}}{dT} \quad (7)$$

$$I_{SC}(T_{cell}, G_{cell}) = I_{SC}(T_0, G_{cell}) + (T_{cell} - T_0) \times \frac{dI_{SC}}{dT} \tag{8}$$

In order to ensure the maximum power output from each of the solar cell, the maximum power point tracking (MPPT) device is connected at the output of CPV module. This ensures that the solar cell operates with maximum possible power output and efficiency, at any operating conditions. Therefore, the MPPT can be modelled by maximizing the expression for cell power output, for which its first derivative is equated to zero [27].

$$\frac{d\dot{P}}{dV} = I_0 \left[\exp\left(\frac{qV}{nkT_{cell}}\right) - 1\right] - I_{SC} = 0 \tag{9}$$

After simplifying the derivative, current and voltage at maximum power point are expressed as [27]

$$V_{MPPT} = V_0 - \frac{nkT_{cell}}{q} \ln(1 + \frac{qV_{MPPT}}{nkT_{cell}}) \tag{10}$$

$$I_{MPPT} = I_0 \left[\exp\left(\frac{qV_{MPPT}}{nkT_{cell}}\right) - 1\right] - I_{SC} \tag{11}$$

And the cell efficiency at maximal power output is derived as

$$\eta_{cell} = \frac{\dot{P}_{max}}{G_{cell} \times A_{cell}} = \frac{V_{MPPT} \times I_{MPPT}}{G_{cell} \times A_{cell}} \tag{12}$$

V-MEMD module. Figure 4 illustrates the schematic of different components for the V-MEMD system. The system performance can be modelled by analyzing heat and mass transfer and heat and mass balances. A detailed model has been reported and validated in our previous publications [30, 31]. Therefore, only the key governing equations will be presented here. The following assumptions are made for the V-MEMD module during operation:

(1) The membrane is able to completely reject the salt, and the produced vapor is salt-free;
(2) Water and vapor properties are constant in each component, and they are determined by the average pressure, temperature and salinity;
(3) The system is well insulated, and there is no heat loss to the ambient.

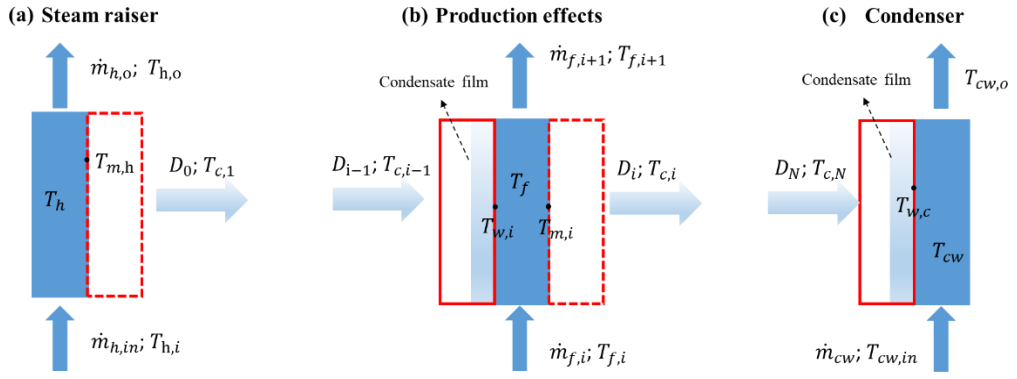

Figure 4. Model schematic for the V-MEMD module, (a) steam raiser, (b) production stages, and (c) condenser

For an N-effect V-MEMD module, mass balances in the steam raiser and the i[th] production effects are summarized as

$$\dot{m}_{h,in} = \dot{m}_{h,o} + \dot{D}_0 \quad (13)$$
$$\dot{m}_{f,i} = \dot{m}_{f,i-1} - \dot{D}_i \quad (14)$$
$$\dot{m}_{f,i}X_i = \dot{m}_{f,i-1}X_{i-1} \quad (15)$$

where $\dot{m}_h$ and $\dot{m}_f$ are the flowrates of the hot water and feed seawater, respectively, and X is the salinity. i is the stage number, while 0 represents the steam raiser. $\dot{D}_0$ and $\dot{D}_i$ are the evaporation rates and they are proportional to the partial vapor pressure difference across the membrane [30, 31]

$$\dot{D}_0 = C_h A_h\{p_{sat}(T_{m,h}) - p_{sat}(T_{c0})\} \quad (16)$$
$$\dot{D}_i = C_h A_{eff}\{p_{sat}(T_{m,i}, X_{m,i}) - p_{sat}(T_{c,i})\} \quad (17)$$

In the above equations, p_{sat} is the saturation vapor pressure, $T_{m,i}$ and $X_{m,i}$ are the temperature and concentration at the membrane surface, respectively, and $T_{c,i}$ is the condensation temperature in the i[th] effect.

The mass transfer coefficient C_h can be calculated using the Knudsen flow model [32]

$$C_h = \frac{2}{3}\frac{\varepsilon r_p}{\tau \delta_m}\left(\frac{8M}{\pi RT}\right)^{0.5} \quad (18)$$

where ε, r_p, τ and δ_m are the porosity, the mean pore radius, the tortuosity, and the thickness of the membrane, respectively. M is the molecular weight of water, R is the universal gas constant, and T_m is the membrane temperature.

Distillate of the first effect is directed back to the hot water tank, while the remaining is collected as freshwater. Thus, overall freshwater productivity is calculated as

$$\dot{D} = \sum_{i=2}^{N} \dot{D}_i \quad (19)$$

Similar to mass balances, heat balances in different components are expressed as

$$\dot{m}_{h,in}H_{h,in} = \dot{m}_{h,o}H_{h,o} + \dot{D}_0 H_g \quad (20)$$
$$\dot{m}_{f,i-1}H_{f,i-1} = \dot{m}_{f,i}H_{f,i} + \dot{D}_i H_g \quad (21)$$
$$\dot{D}_N H_{fg} = \dot{m}_{cw}c_{p,cw}(T_{cw,o} - T_{cw,in}) \quad (22)$$

In the above equations, H is the enthalpy, $\dot{m}_{cw}$ is the cooling water flowrate, H_{fg} is the latent heat of vaporization, $\dot{m}_{cw}$ is the cooling water flowrate and T_{cw} is the cooling water temperature.

In the steam raiser, the latent heat of vaporization is supplied by heat convection. The process is modelled as

$$\dot{D}_0 H_{fg} = h_{mem,h}A_h(T_h - T_{m,h}) \quad (23)$$

where A_h is the heat transfer area in the steam raiser, and T_h and $T_{m,h}$ are the respective temperatures for hot water and membrane. h is the heat transfer coefficient calculated as [33, 34]

$$Nu = \frac{hd}{k} = 0.664K_{dc}Re^{0.5}Pr^{0.33}\left(\frac{d_{h,s}}{l_m}\right)^{0.5} \quad (24)$$

where k is the thermal conductivity, K_{dc} is the correction factor for the spacer-filled geometry, $d_{h,s}$ is the hydraulic diameter for the spacer-filled channel and l_m is the mesh size. Re and Pr are the Reynolds number and Prandtl number, respectively. They are calculated as [35]

$$Re = \frac{ud_{h,s}\rho}{\mu} \tag{25}$$

$$Pr = \frac{c_p\mu}{k} \tag{26}$$

In the above equations, u is the flow velocity, ρ is the liquid density and μ is the dynamic viscosity.

The generated steam condenses on the foil frames and the condensate forms a thin film. The condensation process is modelled as

$$\dot{D}_{i-1}H_{fg} = \frac{k_{film}}{\delta_{film,i}}A_{eff}(T_{c,i-1} - T_{w,i}) \tag{27}$$

with T_c and T_w being the temperatures of vapor and foil, respectively. δ is the film thickness that can be obtained as [35]

$$\delta_{film,i} = \frac{3}{4}\left[\frac{3\mu_w Z_{foil}\dot{D}_{i-1}}{A_{eff}g\rho_l(\rho_l - \rho_v)}\right]^{1/3} \tag{28}$$

where μ_w is the dynamic viscosity of the condensate, Z_{foil} is the height of the plastic foil, g is the gravitational constant, ρ_l is the density of the condensate and ρ_g is the density of the vapor.

In each effect, the condensation heat is transferred from the foils to the feed seawater. The seawater is heated the boiling temperature and partially evaporates. The process is modelled as

$$h_{eff,i}A_{eff}\left(T_{w,i} - T_{f,ave}\right) = \dot{m}_{f,i-1}c_{p,i}\left(T_{f,i} - T_{f,i-1}\right) + \dot{D}_i H_{fg} \tag{29}$$

The vapor produced in the last effect is condensed by the cooling water in the condenser, which is modelled as

$$\dot{D}_N H_{fg} = \frac{k_{film}}{\delta_{film,c}}A_c(T_{c,N} - T_{w,c}) \tag{30}$$

$$\frac{k_{film}}{\delta_{film,c}}A_c(T_{c,N} - T_{w,c}) = h_c A_c\left(T_{w,c} - \frac{T_{cw,in} + T_{cw,o}}{2}\right) \tag{31}$$

where $T_{c,N}$ is the vapor temperature in the condenser, $T_{w,c}$ is the temperature of the PP foil, and A_c is the heat transfer area in the condenser.

Heat storage tank. Mathematical models for the heat storage tank have also been well established and validated in the literature [36, 37]. The tank is divided into several layers in the vertical direction, and each layer is assumed to have a uniform temperature, as shown in *Figure 5*. Coolant stream circulating through the solar collector leaves from the bottom and returns to the top layer, while hot water supplied to the V-MEMD module leaves from the top layer and returns to the bottom layer. Other assumptions for the heat storage tank include:

(1) Hot water in the storage tank is incompressible, and the mass in each control volume remains unchanged;
(2) Water temperatures in each layer are impacted by heat conduction and convection.

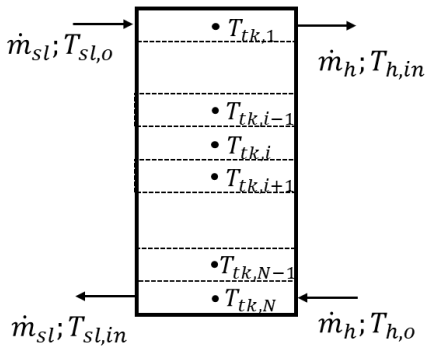

Figure 5. Model schematic for the heat storage tank

The energy balance equations for an intermediate layer is given as [37]

$$\Delta m_i c_p \frac{dT_{tk,i}}{dt} = kA_i \frac{T_{tk,i-1} - T_{tk,i}}{\Delta Z} + kA_i \frac{T_{tk,i+1} - T_{tk,i}}{\Delta Z} + U_{loss} A_i (T_{amb} - T_{tk,i}) + \begin{cases} \dot{m}_{tk} c_p (T_{tk,i-1} - T_{tk,i}), if \ \dot{m}_{sl} > \dot{m}_h \\ \dot{m}_{tk} c_p (T_{tk,i+1} - T_{tk,i}), if \ \dot{m}_{sl} < \dot{m}_h \end{cases} \quad (32)$$

where Δm is the fluid mass in each layer, A is the cross-section area, and ΔZ is the height of the layer. The left terms represents energy change in the i^{th} layer, and the right terms are the energy exhcnage with the surrounding layers and the environment. Specifically, the first two terms on the right side are heat conduction from surrounding layers, the third term is heat loss to the ambient, and the last term represents heat transfer due to convection.

Similarly, energy balances in the top and bottom layers are written as

$$\Delta m_1 c_p \frac{dT_{tk,1}}{dt} = kA_i \frac{T_{tk,2} - T_{tk,1}}{\Delta Z} + \dot{m}_{sl} c_p T_{sl,in} + U_{loss} A_i (T_{amb} - T_{tk,1}) - \dot{m}_h c_p T_{tk,1} \begin{cases} -\dot{m}_{tk} c_p T_{tk,1}, if \ \dot{m}_{sl} > \dot{m}_h \\ \dot{m}_{tk} c_p T_{tk,2}, if \ \dot{m}_{sl} < \dot{m}_h \end{cases} \quad (33)$$

$$\Delta m_N c_p \frac{dT_{tk,N}}{dt} = kA_i \frac{T_{tk,N-1} - T_{tk,N}}{\Delta Z} + kA_i \frac{T_{tk,i+1} - T_{tk,i}}{\Delta Z} + \dot{m}_h c_p T_{ho} - \dot{m}_{sl} c_p T_{tk,N} U_{loss} A_i (T_{amb} - T_{tk,1}) + \begin{cases} \dot{m}_{tk} c_p T_{tk,N-1}, if \ \dot{m}_{sl} > \dot{m}_h \\ -\dot{m}_{tk} c_p T_{tk,N},, if \ \dot{m}_{sl} < \dot{m}_h \end{cases} \quad (34)$$

where $\dot{m}_{sl}$ and $\dot{m}_h$ are the flowrates of hot water circulating through the solar collectors and the V-MEMD module, respectively. $\dot{m}_{tk}$ is the prevailing flow in the vertical direction

$$\dot{m}_{tk} = \begin{cases} \dot{m}_{sl} - \dot{m}_h, if \ \dot{m}_{sl} > \dot{m}_h \\ \dot{m}_h - \dot{m}_{sl}, if \ \dot{m}_{sl} < \dot{m}_h \end{cases} \quad (35)$$

Performance measurement. The performance of the system can be measured using the production rates of electricity and freshwater, as derived previously. In addition, the efficiencies of energy collection, conversion, and utilization are also important. Electrical and thermal conversion efficiencies of the CPV/T module are defined as

$$\eta_{elec} = \frac{\dot{E}}{DNI \times A_{lens}} \times 100\% \quad (36)$$

$$\eta_{th} = \frac{\dot{Q}}{DNI \times A_{lens}} \times 100\% \tag{37}$$

while the energy efficiency of the V-MEMD module is measured using the specific energy consumption for producing a unit mass of freshwater

$$SEC = \frac{\dot{m}_{h,in} H_{h,in} - \dot{m}_{h,o} H_{h,o}}{\dot{D}} \tag{38}$$

In addition to the energy efficiencies, the exergy efficiency is also a powerful measurement of the system's thermodynamic performance. The exergy efficiency of the system can be expressed as the ratio of exergy output to exergy input

$$\eta_{ex} = \frac{\sum \dot{E}_{x,out}}{\sum \dot{E}_{x,in}} \tag{39}$$

where exergy input is the solar radiation, and its value is calculated from the solar radiation (*I*), the ambient temperature (T_{amb}) and the temperature of the sun (T_{sun}) [38]

$$\dot{E}_{x,in} = I A_{lens} [1 - \frac{4}{3}\frac{T_{amb}}{T_{sun}} + \frac{1}{3}(\frac{T_{amb}}{T_{sun}})^4] \tag{40}$$

while exergy output includes exergy of water and electricity

$$\dot{E}_{x,out} = \dot{E} + \dot{D} w_{sep} \tag{41}$$

The least work of separation for desalination, w_{sep}, is calculated as the difference of Gibbs free energy between inlet and outlet streams [39]

$$w_{sep} = g_d + \left(\frac{1}{r} - 1\right) g_b - \frac{1}{r} g_f \tag{42}$$

In the above equation, *g* represents the Gibbs free energy, and *r* is the recovery ratio of the desalination system. Subscripts *d*, *b*, and *f* represent the distillate, brine, and feed seawater. The detailed derivation is available in [39].

3.2 Economic model

To evaluate the economic viability of the system, the levelized cost of freshwater is calculated by considering the initial and operational costs. The generated electricity is assumed to be sold to the grid to cover the initial and operational expenses partially, and the remaining costs are allocated to the produced water. Therefore, the levelized freshwater cost is expressed as

$$c_{water} = \frac{(C_{CPVT} + C_{V-MEMD} + C_{htk}) \times CRF + c_{O\&M} - \sum(\dot{E} - \dot{P}) \times c_{elec}}{\sum \dot{D}} \tag{43}$$

where $\dot{P}$ is the annual electricity consumption of the water circulation pumps and vacuum pump. C_{CPVT} represents the initial cost of the CPV/T collectors and associated auxiliary devices, C_{htk} is the cost of the heat storage tanks, and C_{V-MEMD} is the initial cost of the V-MEMD desalination module. $c_{O\&M}$ is the annual maintenance and operation cost, and c_{elec} is the price of electricity. *CRF* is the capital recovery factor.

CRF is calculated from the interest rate *i* and plant lifespan *n*

$$CRF = \frac{i \times (1+i)^n}{(1+i)^n - 1} \tag{44}$$

The cost of the CPV/T module includes the solar cells and the heat recovery system and is expressed as

$$C_{CPVT} = C_{cell} + C_{hr} \tag{45}$$

while the cost of the V-MEMD module consists of the expenses for pretreatment, membrane, membrane module, feed tank, brine tank and utility.

$$C_{V-MEMD} = C_{pre} + C_{mem} + C_{module} + C_{tank} + C_{utility} \tag{46}$$

The O&M cost covers solar panel maintenance, filtration, brine disposal, chemical, membrane replacement, labor as well as spare cost. It is calculated as

$$c_{O\&M} = c_{panel} + c_{filtration} + c_{brine} + c_{chemical} + c_{spare} + c_{labor} + c_{membrane} \tag{47}$$

3.3 Solution algorithm and model validation

The process model for the proposed cogeneration system is solved using Matlab. At the beginning of the simulation, the initial temperature of the heat storage tank is assumed, and weather data is imported. Based on hot water temperature and solar radiation, solar cell efficiency is calculated. Afterward, electricity and heat generation from the CPV/T module is quantified. Meanwhile, water productivity and energy consumption of the V-MEMD module is calculated using the algorithm developed previously in [30, 31]. Based on heat generation and consumption, hot water temperature in the heat storage tank is updated and employed for the next time step. The process is repeated until the desired time span is reached. The solution algorithm is depicted in Figure 6.

Mathematical models for the solar cell and the V-MEMD module are validated using experimental data, while the heat storage tank model is compared with data reported in the literature [40]. Average discrepancies between experimental data and model prediction, expressed as root-mean-square-error (RSME), are below 6%. The detailed validation process is provided in the *Supplementary Material*.

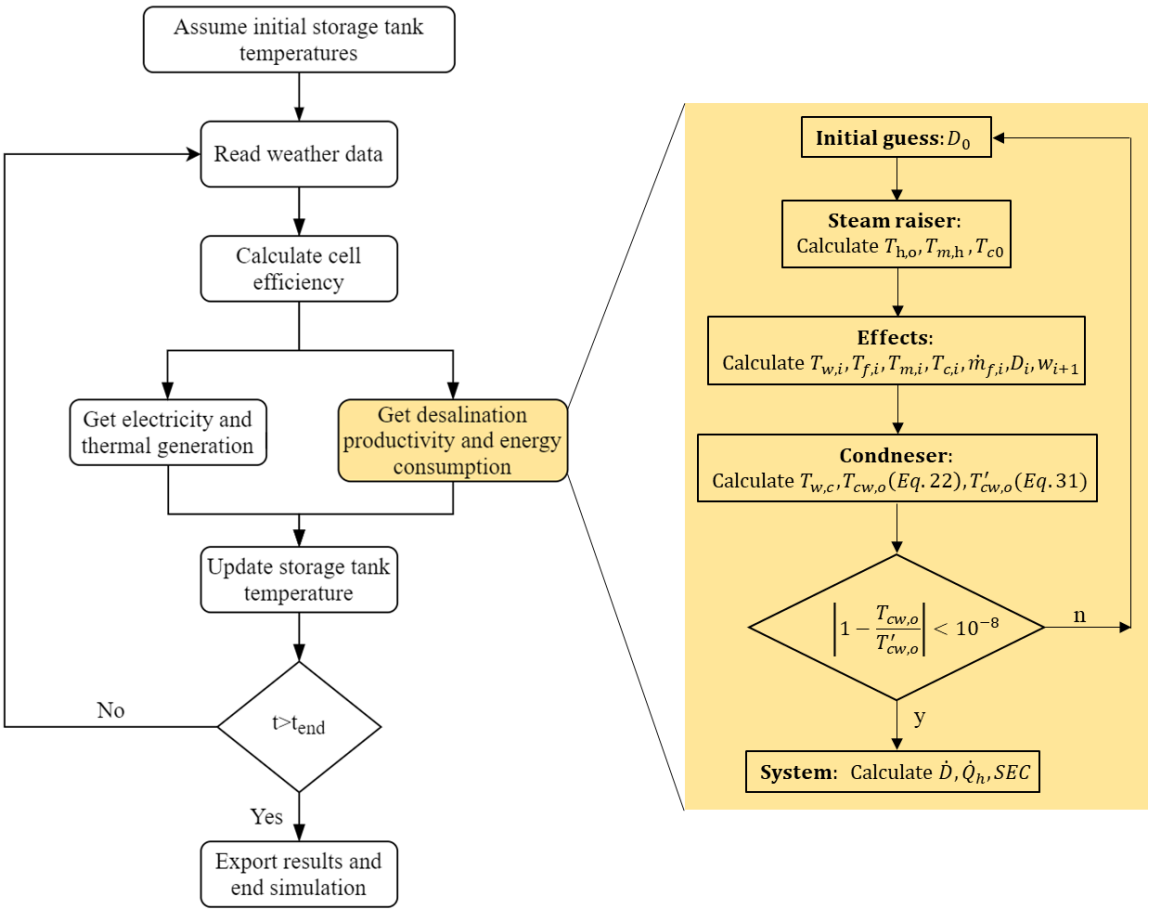

Figure 6. Schematic of the solution algorithm

4. Results and discussion

This section presents the thermodynamic and economic performance of the proposed system. Since both CPV/T and V-MEMD units have been evaluated in the previous studies, the current study will focus on the performance of the integrated system. Firstly, the productivity of freshwater and electricity will be presented and discussed. Afterward, the overall exergy efficiency will be evaluated under different design and operating conditions. Based on the productivity information, the levelized cost of freshwater will be calculated and analyzed.

4.1 Electricity & water output

Without loss of generality, a solar field with a collector area of 8 m^2 is considered. The hot water flowrates in the solar collectors and the steam raiser are initially set as 9 LPM, and the feed seawater flowrate is 0.3 LPM. Dimensions of the heat storage tank are assumed to be D 0.5 m × H 1 m, while the size of the freshwater tank will be achieved later based on the production profile. The annual climatic data for Makkah, Saudi Arabia, will be employed as the model input. To avoid unnecessary pumping power consumption, water circulation through the solar cells is paused when solar radiation is zero, and the V-MEMD module

is operated only when the temperature difference between the hot water and the ambient is higher than 20 ℃. Other considerations and simplifications in the simulations include:

(1) The cell temperature is 10 ℃ higher than the circulating fluid outlet temperature [41];
(2) The hot water tank has a uniform temperature of 70 ℃ at the beginning of the simulations;
(3) The pumping power consumption of the V-MEMD module is 5 kWh for producing per m^3 of distillate, and it is provided by the CPV/T module.

It should be noted that pumping power consumption of the MEMSYS module is measured to be 5-20 kWh/m^3 [42]. However, the value doesn't represent its final performance, since the module is not optimized in terms of pumping power consumption [21, 42]. Currently, the module has a small capacity, and the pumps are inefficient. Also, redundant pumps are operating within the system. An improved V-MEMD module will have lower electricity consumption, and the value of 5 kWh/m^3 represents a realistic estimation.

Figure 7(a) shows the solar radiation and the ambient temperature on a typical sunny day. The solar radiation value is close to 1000 W/m^2 from 10:00 am to 3:00 pm. Such a high solar intensity results in a significant ambient temperature fluctuation (>13 ℃). The hot water temperature in the heat storage tank is also presented in Figure *7*(a). Its value increases from 7:00 am to 4:00 pm, indicating the storage of excessive thermal energy after heat input to the V-MEMD module. For the remaining hours of the day, the collected solar heat is insufficient for desalination application, and the hot water temperature decreases. Figure *7*(b) shows the water productivity and electricity output for each hour. Electricity output follows exactly the trend of solar radiation, while water productivity is relatively stable for the whole day due to the buffering effect of the hot water tank. A small peak of water production (~7 L/hr) is observed at 5:00 pm. This is because the ambient temperature drops significantly after sunset, while the hot water temperature is still high.

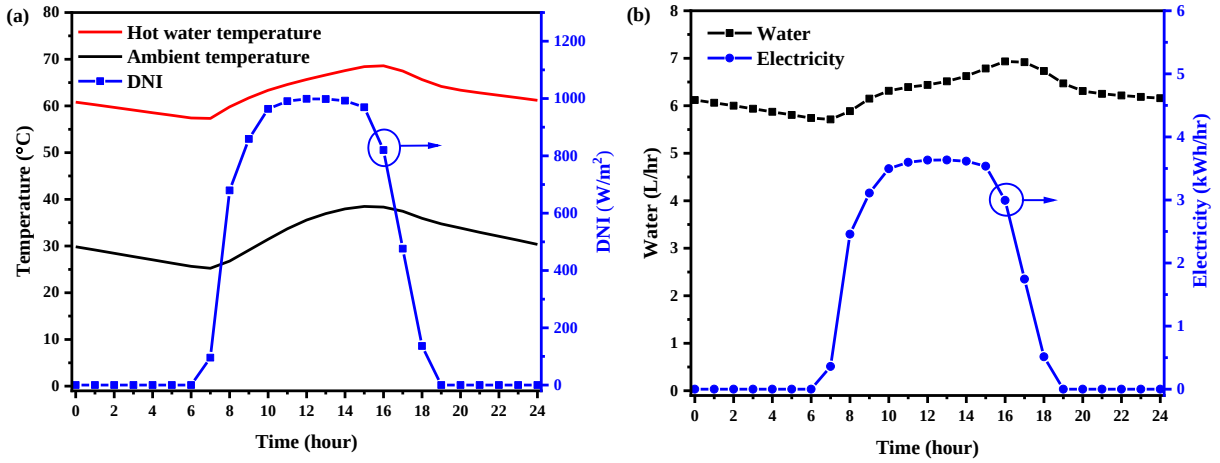

Figure 7. Daily profile of (a) solar radiation and water temperatures, and (b) water production rate and electricity generation on a typical day (Oct-15)

Table 1 summarizes the system performance on a monthly basis. The results are calculated using the annual weather data. Detailed profiles of temperature and solar intensity are provided in the *Supplementary Material*. It is clearly shown in the table that both electrical and thermal efficiencies are stabilized throughout the year. The monthly average electricity efficiency is ~24%, and the thermal efficiency is ~45%. This is attributed mainly to the high solar intensity, which falls into the range where cell efficiency is no longer sensitive to solar concentration. Also, the variation of the cell temperature is marginal due to effective thermal management by the heat storage tank. As a result of stable electrical and thermal

efficiencies, the productivity of both electricity and freshwater is proportional to solar radiation. The peak value of electricity generation (514.16 kWh/month) is observed in October when solar radiation is maximal at 275.48 kWh/month/m^2, while the amount is small from June to August due to a relatively lower solar intensity. Similarly, water productivity is also maximized in October. However, the minimal water production rate occurs in February (2.67 m^3/month) instead of the summer months. The reason is that the ambient temperature in February is the lowest (25.02 ℃), leading to additional energy consumption to heat the intake seawater to the boiling temperature.

Table 1. Summary of monthly performance and weather data for the proposed system with 8 m^2 collector area

Month	DNI (kWh/month/m^2)	T_{amb} (℃)	Water (m^3/month)	Electricity (kWh/month)	η_{elec} (%)	η_{th} (%)	η_{cell} (%)	SEC (kWh/m^3)
Jan	177.15	26.14	3.06	337.06	24.86	45.01	36.83	222.91
Feb	165.83	25.02	2.67	316.48	24.86	45.01	36.83	224.78
Mar	213.16	27.49	3.44	405.12	24.76	45.11	36.69	219.87
Apr	224.45	30.48	3.76	422.89	24.60	45.29	36.44	215.21
May	207.02	33.83	3.53	388.36	24.52	45.37	36.32	212.15
Jun	162.57	35.10	2.79	303.91	24.44	45.45	36.21	211.98
Jul	163.11	35.49	2.84	304.27	24.40	45.49	36.16	210.95
Aug	163.70	35.01	2.78	306.59	24.47	45.42	36.25	211.72
Sep	194.36	33.67	3.32	364.82	24.53	45.36	36.34	212.34
Oct	275.48	31.43	4.72	514.16	24.40	45.49	36.15	212.29
Nov	253.18	27.96	4.27	476.02	24.56	45.33	36.38	216.66
Dec	192.97	25.73	3.16	367.91	24.86	45.01	36.82	222.99

Figure 8 visualizes the annual energy flow of the system, including energy collection, utilization, and losses. Among the overall solar input, 25% is lost in the optical devices (Fresnel lenses and homogenizers), and the rest reaches the solar cells. 33% of the solar radiation reaching the cell surface is converted into electricity. 10% of the produced electricity is lost in the DC/AC inverter, and 4% is consumed by the pumps, leading to a final electricity output of 562 kWh for the unit collector area. The remaining radiation is mostly converted into heat and transferred to the circulating fluid. Most of the collected heat (1078 kWh/m^2-year) is utilized to drive the desalination process, and a tiny amount is stored in the hot water tank. The annual freshwater production rate is 42 m^3 (5.25 m^3 per m^2 collector area), and the corresponding desalination efficiency is 205 kWh/m^3. It is also worth mentioning that nearly 70% of the solar radiation is effectively collected and utilized in the current system (24.6% electricity and 45.3% thermal). Although well-designed solar thermal collectors can also achieve such a high conversion efficiency, they only produce low-grade heat, whose energy quality is much lower than electricity.

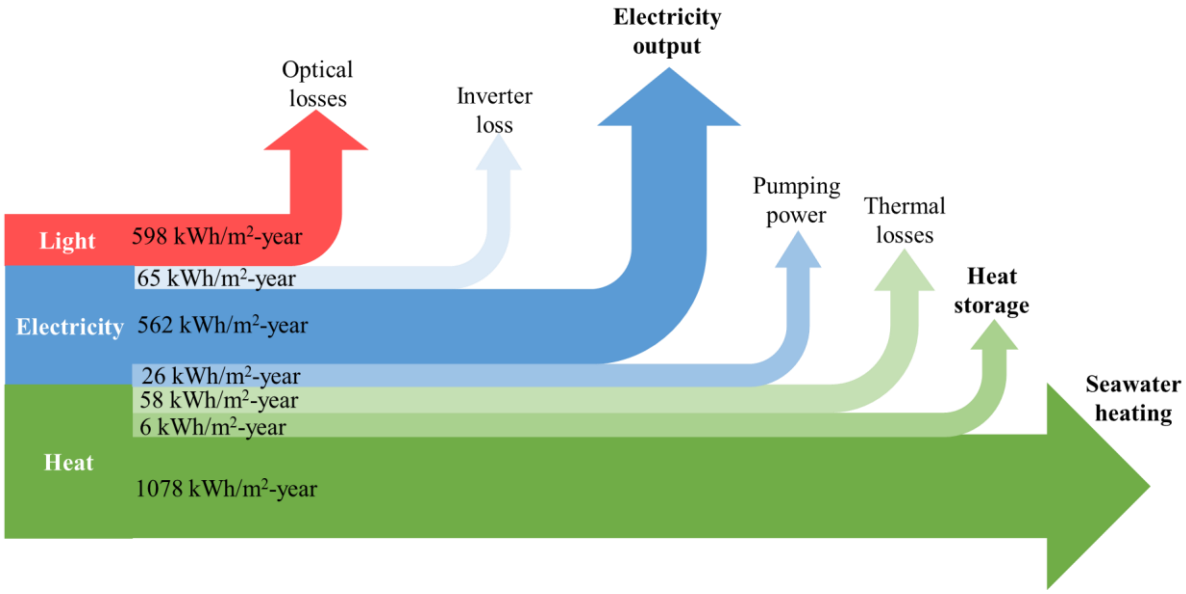

Figure 8. Energy collection, utilization, and losses diagram for the proposed system on an annual basis

Figure 9 shows the annual profile of freshwater in the storage tank. Initial water storage and daily water consumption are assumed to be 2230 L and 110 L/day, respectively. As shown in the figure, the amount of water in the storage tank increases from March to May as well as from September to November, since water productivity is higher than consumption in these months. For the rest of the year, water production is lower, and stored freshwater is consumed. It is worth mentioning that the tank never runs out of storage (minimum water volume is 8 L), indicating that the system is able to provide an uninterrupted water supply throughout the year. On the other hand, the maximum volume of stored water is 2549 L, which will be the freshwater tank's minimum volume to provide an uninterrupted water supply.

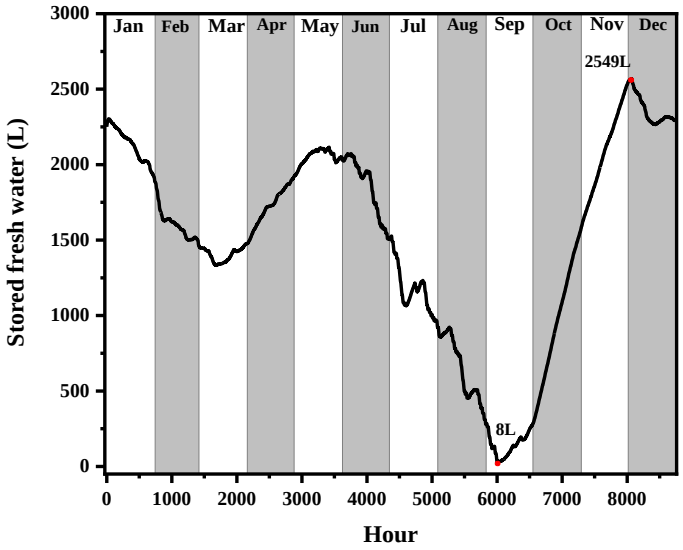

Figure 9. Annual profile of stored freshwater

The system performance is expected to vary when cell efficiency is different. Under a given weather condition, the cell efficiency is determined by the cell temperature, which can be rehulated by the flowrates

of the hot water and the feed seawater as well as the dimension of the hot water tank. Figure 10(a) shows the impact of the hot water flowrate on water and electricity production rates. For optimal operation of the V-MEMD module, the feed seawater flowrate is controlled to be 1/30 of the hot water flowrate [30]. Therefore, the increase of hot water flowrate represents a larger desalination capacity, and more heat will be extracted from the storage tank. Consequently, temperatures of hot water and the solar cells will be lower, leading to higher cell efficiency and more electricity output. In contrast, water productivity has a peak value under a hot water flowrate of 9.6 LPM due to the combined impacts of several factors. Firstly, when more solar radiation is converted into electricity under a higher hot water flowrate, less heat is harvested for desalination application, as revealed by a lower thermal efficiency (plotted in Figure 10(b)). Moreover, specific energy consumption for the V-MEMD module is higher under a lower hot water temperature [30]. Reduced heat supply and lower heat efficiency both have adverse effects on water productivity. On the other hand, heat loss to the ambient is also minimized when hot water temperature is lower, which promotes water production. The optimal value of 9.6 LPM is the result of best trade-off among these conflicting factors.

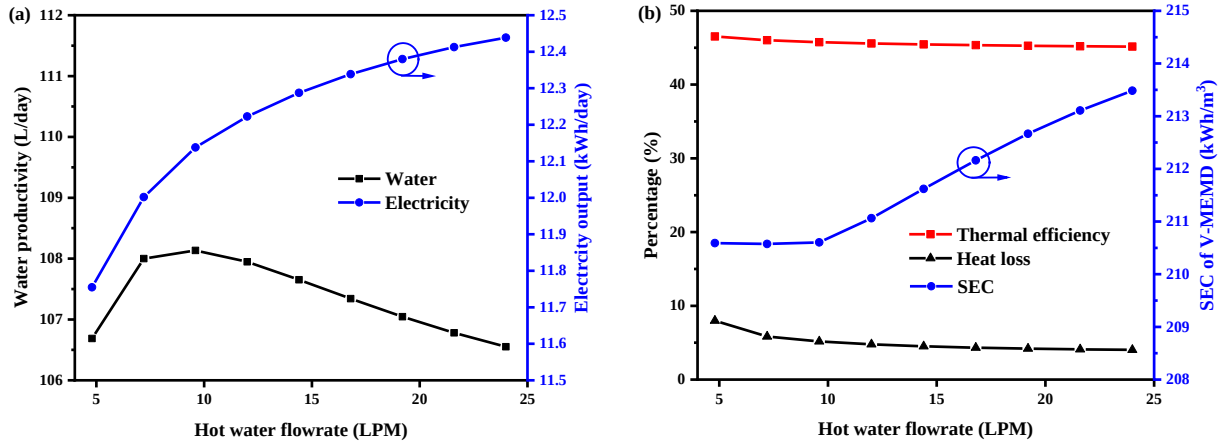

Figure 10. Effect of hot water flowrate on (a) water productivity and electricity generation, and (b) thermal efficiency, heat loss and desalination SEC. The storage tank diameter is 0.5 m, and the feed water flowrate is 1/30 of the hot water flowrate.

Figure 11 summarizes the system performance under different seawater flowrates. Here the hot water flowrate is fixed at 9.6 LPM. As shown in Figure 11(a), electricity output is marginally improved by ~2% (0.3 kWh/day) when increasing the feed flowrate from 0.15 to 0.46 LPM, while water productivity suffers a considerable drop of 18% (20 L/day). Under the flowrate range considered, the change of hot water temperature is marginal, and conversion efficiencies (electricity and thermal) of the CPV/T module and heat loss to the ambient are relatively stable, which can be seen from Figure 11(b). The only parameter that is significantly impacted by the feed flowrate is the energy efficiency of the V-MEMD module. When the feed flowrate is higher, more heat is consumed for pre-heating the feed seawater to the evaporation temperature [30], leading to lower thermal efficiency and smaller freshwater productivity.

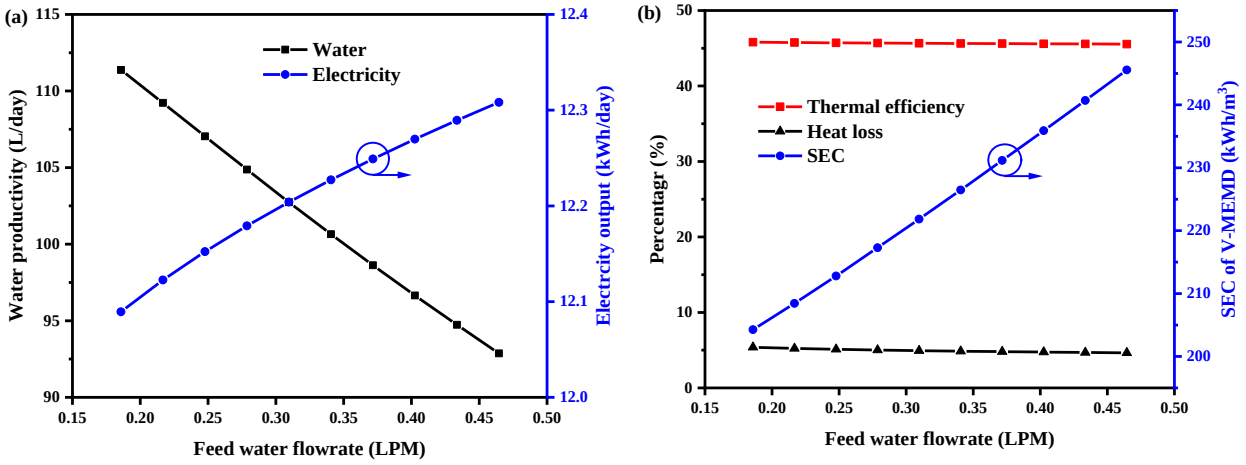

Figure 11. Effect of feed water flowrate on (a) water productivity and electricity generation, and (b) thermal efficiency, heat loss and desalination SEC. Hot water flowrate is 9.6 LPM, and the tank diameter is 0.5 m

The heat storage tank dimension is also expected to affect the cell temperature and change system performance, as presented in Figure 12. The tank is designed to have a height-diameter ratio of 2, and its diameter is provided here to represent its dimension. It is clear from Figure 12(a) that a larger tank will promote electricity generation while reducing water production. When the tank diameter is enlarged from 0.5 to 1.5 m, freshwater productivity drops by 40%, while electricity generation is promoted by 4.6%. This is because a larger tank has better temperature regulation capability, leading to lower temperatures for cells and hot water. A lower cell temperature promotes electricity generation while reducing thermal energy harvesting. Meanwhile, heat loss becomes more significant when the tank is larger. As plotted in Figure 12(b), only 5% of collected heat is lost when the tank diameter is 0.5 m, while the value becomes 36% for a tank diameter of 1.5 m. Reduced heat collection and more heat loss results in low freshwater productivity under large tank diameters.

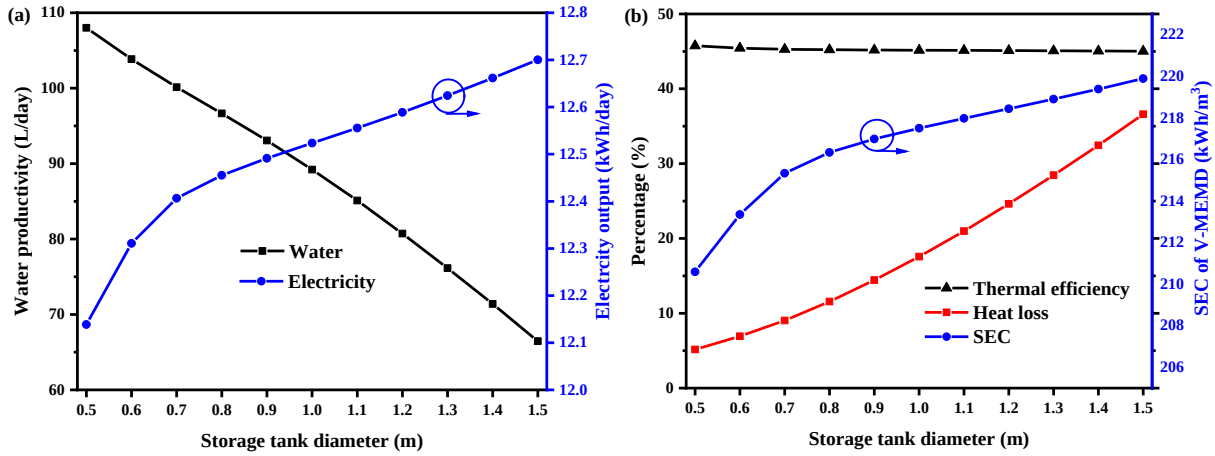

Figure 12. Effect of storage tank diameter on (a) water productivity and electricity generation, and (b) thermal efficiency, heat loss and desalination SEC. Hot water flowrate is 9.6 LPM, and feed flowrate is 0.3 LPM

Table 2 compares the annual performance of the proposed system in several cities that are facing water scarcity. For simplicity, the system is designed to have 8 m^2 solar collector area and 4 V-MEMD stages. It should be noted that the optimal design will vary under different weather conditions. Generally, the productivity of electricity and freshwater are proportional to solar intensity, while the ambient temperature also has an impact on the system performance. For cities with higher ambient temperatures (e.g., Makkah and Singapore), the cell efficiency is lower, leading to less electricity output, more heat generation and more water production. On the other hand, electricity production is enhanced while water productivity decreases when the ambient temperature is lower, as can be seen from the performance data of Shanghai and Melbourne.

Table 2. Annual performance of the proposed system in different cities

City	DNI (kWh/year/m^2)	T_{amb} (°C)	Water (m^3/year)	Electricity (kWh/year)	η_{elec} (%)	η_{th} (%)	η_{cell} (%)	SEC (kWh/m^3)
Makkah	2392.97	30.64	41.32	4737.90	24.75	45.13	36.67	218.13
Singapore	892.50	26.62	16.29	1771.55	24.81	45.06	36.76	226.59
Shanghai	833.12	15.77	14.46	1667.94	25.03	44.83	37.07	244.17
Abu Dhabi	1612.36	26.73	25.13	3173.40	26.55	45.28	39.34	217.64
Cairo	1968.23	21.32	29.97	3890.82	26.63	45.17	39.46	223.04
Melbourne	1352.60	14.00	18.85	2681.36	26.66	45.09	39.49	233.79

4.2 Exergy efficiency

From the above discussions, it can be found that the design and operating parameters usually have conflicting effects on electricity generation and water productivity. To enable a more in-depth analysis of these parameters, the exergy of all output streams is calculated to obtain the overall system efficiency, and the results are plotted in Figure 13. Interestingly, the system's exergy efficiency is stabilized between 25-27%, despite of large fluctuations in water productivity with design and operating conditions. This is because the collected heat is of low grade and its exergy value is much lower than that of electricity. Moreover, further destruction of exergy occurs in the desalination process. Consequently, the freshwater's exergy content is very small, and it contributes to <1% of the exergy output. The overall exergy efficiency is dominated by electricity conversion efficiency, which has marginal change under different conditions. Therefore, the impacts of different parameters on exergy efficiency are insignificant.

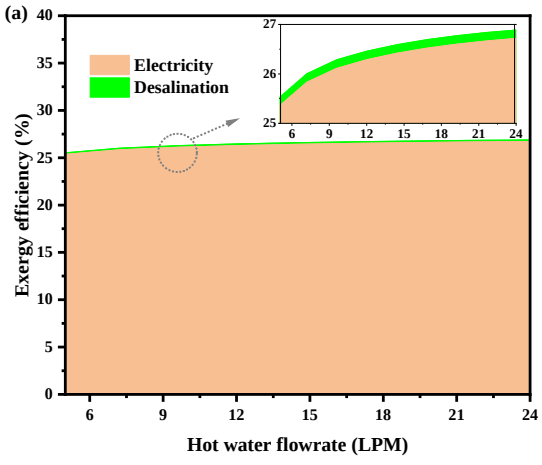

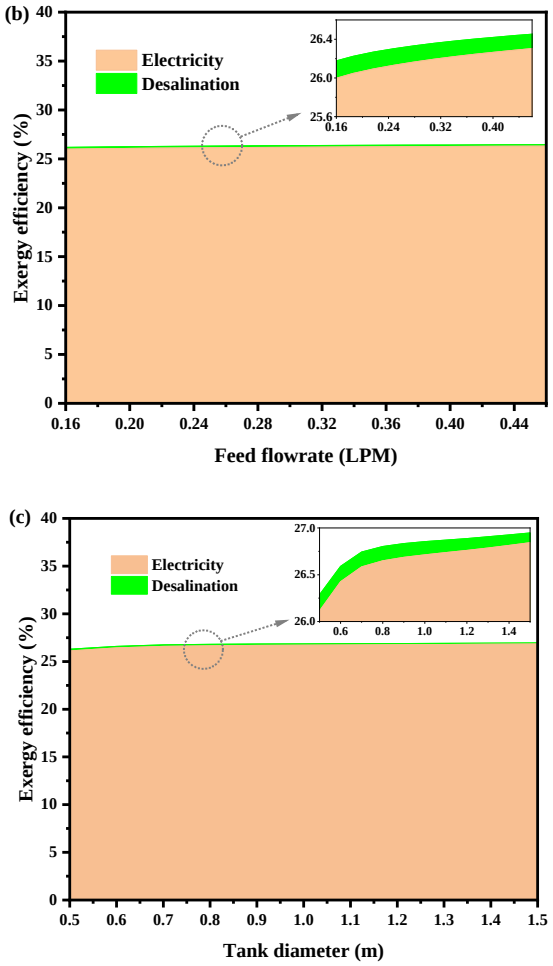

Figure 13. Exergy efficiency of the system under different (a) hot water flowrate, (b) feed flowrate and (c) tank diameter

4.3 Economic analysis

Based on the annual productivity of electricity and freshwater, this section evaluates the proposed system's economic performance. *Table 3* summarizes the economic data used in the analysis. They are obtained from the literature published in peer-reviewed journals and the quotations provided by the contractors and suppliers. A wide range of solar panel costs and electricity prices are evaluated to cover different local market conditions and possible public funding and feed-in tariffs for solar energy.

Table 3. Economic data and assumptions employed in the model

Initial cost	
CPV module with tracking	\$300-500/m^2
Thermal recovery [41, 43]	10% of CPV module
Pretreatment [44]	\$79.25/(m^3/day)
Membrane [45]	\$60/m^2
Membrane module [45]	\$103/(m^3/day)
Water tank [46]	\$21.14/m^3

Utility cost [46]	\$42.27(m^3/day)
Plant lifespan	20 years
Interest rate	2%
O&M cost	
Solar plant maintenance [27]	2% of initial plant cost
Filtration [45]	\$0.0132/m^3
Brine disposal [45]	0.0015/m^3
Chemical cost [47]	\$0.018/m^3
Spares cost [45]	\$0.033/m^3
Labor cost [48]	\$0.03/m^3
Membrane replacement	10%/year
Electricity price	\$0.02-0.08/kWh

Figure 14 plots the life-cycle cost for freshwater expressed in \$/m^3. The water cost is proportional to the solar panel price, while inversely proportional to the electricity price. Under high electricity prices and low solar panel costs, the water cost has negative values, as highlighted in the gray region. This is when the revenue of selling the electricity is higher than the costs of the CPV/T system and the desalination module. It should be noted that the regular electricity price in Saudi Arabia is \$0.05/kWh, and solar panel price ranges \$300-500/m^2 in the market. The corresponding desalination cost is \$0.7-4.3/m^3, which is comparable to large-scale solar desalination systems (\$4-10/m^3 for solar-driven membrane distillation [49], \$2-2.5/m^3 for solar MED [49] and >\$3/m^3 for solar MSF [50]). Therefore, the proposed system will be economically viable and competitive.

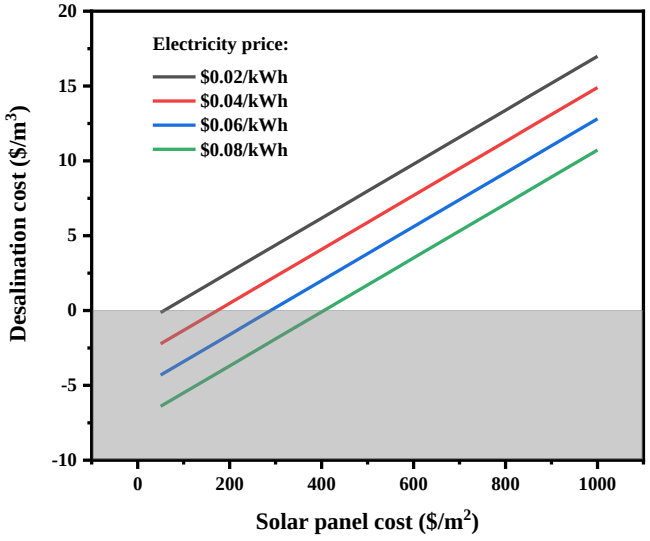

Figure 14. Freshwater cost under different solar panel costs and electricity prices

5. Conclusions

A decentralized solar cogeneration system integrating concentrated photovoltaic/thermal (CPV/T) collectors and vacuum multi-effect membrane distillation (V-MEMD) has been evaluated. The system is

compact and enables decentralized applications such as rooftop installation. To evaluate the potential of the proposed system, a thermodynamic analysis is firstly conducted to obtain its productivity and energy efficiency, followed by an economic analysis. Key findings that emerged from this study include:

(1) The electricity and thermal efficiencies of the CPV/T module are stable throughout the year (25% and 45%, respectively), making the electricity output proportional to the solar irradiance. Freshwater production rate is impacted by the ambient temperature, with a lower ambient temperature leading to lower water productivity;
(2) The CPV/T module is able to convert ~70% of solar energy into useful effects, including heat and electricity. The majority of energy losses occurs in the optical components;
(3) A higher flowrate for hot water and feed seawater and a larger storage tank volume will lower cell temperature, thus promoting electricity generation while degrading freshwater production. The change in water yield is more pronounced than that of electricity output;
(4) The exergy efficiency of the system is dominated by electricity generation, and its value is stabilized at 25-27% under different design and operating conditions;
(5) The life-cycle water cost is \$0.7-4.3/m^3, which is proportional to the solar panel cost while inversely related to the electricity price. When public funding and feed-in tariff are available, the proposed system is profitable and competitive.

The derived results enable in-depth understanding of the proposed water/electricity cogeneration system and provide useful information for future design and operation. To make the system more competitive and appealing, future work will focus on (i) improving the V-MEMD module to reduce its electricity and heat consumption, (ii) designing, commissioning and testing a pilot plant to demonstrate the actual potential, and (iii) optimizing the system design under different weather conditions.

Nomenclature

A	Area, m^2
a	Fitting parameter for solar cell efficiency
C	Cost, \$
C_h	Mass transfer coefficient, s/m
c	Specific cost, \$/kWh or \$/m^3
c_p	Specific heat, J/kg
CPV/T	Concentrated photovoltaic/thermal
CRF	Capital recovery factor
CSP	Concentrated solar power
$\dot{D}$	Distillate flux, kg/s
D	Accumulated distillate mass, kg
d	Diameter, m; diffusion coefficient, m^2/s
DNI	Direct normal irradiance, W/m^2
$\dot{E}$	Electricity, W
G	Solar radiation, W/m^2
g	Gibbs free energy, J/kg
H	Enthalpy, J/kg;
h	Heat transfer coefficient, W/m^2-K
HDH	Humidification-dehumidification desalination

I	Current, A
k	Thermal conductivity, W/m-K; Boltzman's constant
k_{dc}	Correction factor
l	Mesh size, m
m	Mass flowrate, kg/s
M	Molecular weight, g/mol
MD	Membrane distillation
MED	Multi-effect distillation
MJC	Multi-junction cell
MPPT	Maximum power point tracking
MSF	Multi-stage flash desalination
n	Diode ideality factor
Nu	Nusselt number
p	Pressure, Pa
$\dot{P}$	Pumping power, W; electrical power, W
Pr	Prandtl number
PV	Photovoltaic
PV/T	Integrated photovoltaic/thermal
$\dot{Q}$	Heat, W
q	Electrical charge, Coulomb
r	Pore radius, m; recovery ratio, %
R	Universal gas constant, J/mol-K
Re	Reynolds number
RO	Reverse osmosis
SEC	Specific energy consumption, kWh/m^3
T	Temperature, °C
t	Time, s
u	Velocity, m/s
U	Heat loss coefficient, W/m^2-K
VMD	Vacuum membrane distillation
V-MEMD	Vacuum multi-effect membrane distillation
w	Work of separation, J/kg
X	Salt concentration, kg/kg
Z	Height, m

Subscripts

amb	Ambient
ave	Average
b	Brine
c	Condensation
cell	Solar cell
cw	Cooling water
d	Distillate
eff	Effect

elec	Electricity
ex	Exergy
f	Feed
fg	Latent heat
film	Film
g	Gas phase
h	Hot water; heating
htk	Heat storage tank
hr	Heat recovery module
i	ith effect; interest rate, %
in	Inlet
l	Liquid phase
lens	Lens
loss	Energy loss
m	Membrane; mass transfer
max	Maximum
mem	Membrane
N	Number of effect
o	Outlet
O&M	Operation and maintenance
OC	Open circuit
opt	Optical
out	Outlet
p	Pore
sat	Saturation
SC	Short circuit
sep	Separation
sl	Solar
th	Thermal
tk	Tank
w	Plastic foil wall

Greek letters

Δ	Difference
μ	Dynamic viscosity, Pa·s
δ	Thickness, m
ε	Porosity; void fraction
η	Efficiency, %
ρ	Density, kg/m^3
τ	Tortuosity

Acknowledgement

This research was supported by the Water Desalination and Reuse Center (WDRC), King Abdullah University of Science and Technology (KAUST).

References

[1] Footprint, F.W., Food, and A.O.o.t.U. Nations, *Toolkit: Reducing the Food Wastage Footprint*. 2013: Food Agriculture Organization (FAO).

[2] Ferroukhi, R., D. Nagpal, A. Lopez-Peña, T. Hodges, R. Mohtar, B. Daher, S. Mohtar, and M. Keulertz, *Renewable energy in the water, energy & food nexus.* IRENA, Abu Dhabi, 2015.

[3] Chen, Q., S. Oh, Y. Li, and M.K. Ja, *Thermodynamic optimization of a low-temperature desalination system driven by sensible heat sources.* Energy, 2020. **192**: p. 116633.

[4] Hamrang, F., A. Shokri, S. Mahmoudi, B. Ehghaghi, and M.A. Rosen, *Performance Analysis of a New Electricity and Freshwater Production System Based on an Integrated Gasification Combined Cycle and Multi-Effect Desalination.* Sustainability, 2020. **12**(19): p. 7996.

[5] Mohammadi, K., J.G. McGowan, and K. Powell, *Thermoeconomic analysis of a multigeneration system using waste heat from a triple power cycle.* Applied Thermal Engineering, 2021: p. 116790.

[6] Iodice, P., G. Langella, and A. Amoresano, *Modeling and energetic-exergetic evaluation of a novel screw expander-based direct steam generation solar system.* Applied Thermal Engineering, 2019. **155**: p. 82-95.

[7] Iodice, P., G. Langella, and A. Amoresano, *Energy performance and numerical optimization of a screw expander–based solar thermal electricity system in a wide range of fluctuating operating conditions.* International Journal of Energy Research, 2020. **44**(3): p. 1858-1874.

[8] Askari, I.B. and M. Ameri, *Techno economic feasibility analysis of Linear Fresnel solar field as thermal source of the MED/TVC desalination system.* Desalination, 2016. **394**: p. 1-17.

[9] Li, C., G. Kosmadakis, D. Manolakos, E. Stefanakos, G. Papadakis, and D. Goswami, *Performance investigation of concentrating solar collectors coupled with a transcritical organic Rankine cycle for power and seawater desalination co-generation.* Desalination, 2013. **318**: p. 107-117.

[10] Soomro, M.I. and W.-S. Kim, *Performance and economic investigations of solar power tower plant integrated with direct contact membrane distillation system.* Energy conversion and management, 2018. **174**: p. 626-638.

[11] Iaquaniello, G., A. Salladini, A. Mari, A. Mabrouk, and H. Fath, *Concentrating solar power (CSP) system integrated with MED–RO hybrid desalination.* Desalination, 2014. **336**: p. 121-128.

[12] Eltawil, M.A. and Z. Omara, *Enhancing the solar still performance using solar photovoltaic, flat plate collector and hot air.* Desalination, 2014. **349**: p. 1-9.

[13] Yari, M., A. Mazareh, and A. Mehr, *A novel cogeneration system for sustainable water and power production by integration of a solar still and PV module.* Desalination, 2016. **398**: p. 1-11.

[14] Pounraj, P., D.P. Winston, A. Kabeel, B.P. Kumar, A.M. Manokar, R. Sathyamurthy, and S.C. Christabel, *Experimental investigation on Peltier based hybrid PV/T active solar still for enhancing the overall performance.* Energy conversion and management, 2018. **168**: p. 371-381.

[15] Gabrielli, P., M. Gazzani, N. Novati, L. Sutter, R. Simonetti, L. Molinaroli, G. Manzolini, and M. Mazzotti, *Combined water desalination and electricity generation through a humidification-dehumidification process integrated with photovoltaic-thermal modules: Design, performance analysis and techno-economic assessment.* Energy Conversion and Management: X, 2019. **1**: p. 100004.

[16] Anand, B. and T. Srinivas, *Performance evaluation of photovoltaic/thermal–HDH desalination system.* Applied Solar Energy, 2017. **53**(3): p. 243-249.

[17] Giwa, A., H. Fath, and S.W. Hasan, *Humidification–dehumidification desalination process driven by photovoltaic thermal energy recovery (PV-HDH) for small-scale sustainable water and power production.* Desalination, 2016. **377**: p. 163-171.

[18] Chen, Q., M.K. Ja, Y. Li, and K. Chua, *Evaluation of a solar-powered spray-assisted low-temperature desalination technology.* Applied energy, 2018. **211**: p. 997-1008.

[19] Zhao, K., W. Heinzl, M. Wenzel, S. Büttner, F. Bollen, G. Lange, S. Heinzl, and N. Sarda, *Experimental study of the memsys vacuum-multi-effect-membrane-distillation (V-MEMD) module.* Desalination, 2013. **323**: p. 150-160.

[20] Burhan, M., M.W. Shahzad, D. Ybyraiymkul, S.J. Oh, N. Ghaffour, and K.C. Ng, *Performance investigation of MEMSYS vacuum membrane distillation system in single effect and multi-effect mode.* Sustainable Energy Technologies and Assessments, 2019. **34**: p. 9-15.

[21] Zaragoza, G., A. Ruiz-Aguirre, and E. Guillén-Burrieza, *Efficiency in the use of solar thermal energy of small membrane desalination systems for decentralized water production.* Applied Energy, 2014. **130**: p. 491-499.

[22] Chafidz, A., S. Al-Zahrani, M.N. Al-Otaibi, C.F. Hoong, T.F. Lai, and M. Prabu, *Portable and integrated solar-driven desalination system using membrane distillation for arid remote areas in Saudi Arabia.* Desalination, 2014. **345**: p. 36-49.

[23] Andrés-Mañas, J., L. Roca, A. Ruiz-Aguirre, F. Acién, J.D. Gil, and G. Zaragoza, *Application of solar energy to seawater desalination in a pilot system based on vacuum multi-effect membrane distillation.* Applied Energy, 2020. **258**: p. 114068.

[24] Mohammadi, K., S. Khanmohammadi, H. Khorasanizadeh, and K. Powell, *A comprehensive review of solar only and hybrid solar driven multigeneration systems: Classifications, benefits, design and prospective.* Applied Energy, 2020. **268**: p. 114940.

[25] Burhan, M., Q. Chen, M.W. Shahzad, D. Ybyraiymkul, F.H. Akhtar, and K.C. Ng, *Innovative concentrated photovoltaic thermal (CPV/T) system with combined hydrogen and MgO based storage.* International Journal of Hydrogen Energy, 2020.

[26] Ong, C.L., W. Escher, S. Paredes, A. Khalil, and B. Michel, *A novel concept of energy reuse from high concentration photovoltaic thermal (HCPVT) system for desalination.* Desalination, 2012. **295**: p. 70-81.

[27] Burhan, M., K.J.E. Chua, and K.C. Ng, *Sunlight to hydrogen conversion: Design optimization and energy management of concentrated photovoltaic (CPV-Hydrogen) system using micro genetic algorithm.* Energy, 2016. **99**: p. 115-128.

[28] Burhan, M., M.W. Shahzad, and K.C. Ng, *Long-term performance potential of concentrated photovoltaic (CPV) systems.* Energy conversion and management, 2017. **148**: p. 90-99.

[29] Nishioka, K., T. Takamoto, T. Agui, M. Kaneiwa, Y. Uraoka, and T. Fuyuki, *Annual output estimation of concentrator photovoltaic systems using high-efficiency InGaP/InGaAs/Ge triple-junction solar cells based on experimental solar cell's characteristics and field-test meteorological data.* Solar Energy Materials and Solar Cells, 2006. **90**(1): p. 57-67.

[30] Chen, Q., B. Muhammad, F.H. Akhtar, D. Ybyraiymkul, W.S. Muhammad, Y. Li, and K.C. Ng, *Thermo-economic analysis and optimization of a vacuum multi-effect membrane distillation system.* Desalination, 2020. **483**: p. 114413.

[31] Chen, Q., M.K. Ja, Y. Li, and K. Chua, *Thermodynamic optimization of a vacuum multi-effect membrane distillation system for liquid desiccant regeneration.* Applied energy, 2018. **230**: p. 960-973.

[32] Diban, N., O.C. Voinea, A. Urtiaga, and I. Ortiz, *Vacuum membrane distillation of the main pear aroma compound: Experimental study and mass transfer modeling.* Journal of Membrane Science, 2009. **326**(1): p. 64-75.

[33] Da Costa, A., A. Fane, and D. Wiley, *Spacer characterization and pressure drop modelling in spacer-filled channels for ultrafiltration.* Journal of membrane science, 1994. **87**(1-2): p. 79-98.

[34] Phattaranawik, J., R. Jiraratananon, A. Fane, and C. Halim, *Mass flux enhancement using spacer filled channels in direct contact membrane distillation.* Journal of membrane science, 2001. **187**(1-2): p. 193-201.

[35] Rohsenow, W.M., J.P. Hartnett, and Y.I. Cho, *Handbook of heat transfer*. Vol. 3. 1998: McGraw-Hill New York.

[36] Nash, A.L., A. Badithela, and N. Jain, *Dynamic modeling of a sensible thermal energy storage tank with an immersed coil heat exchanger under three operation modes.* Applied energy, 2017. **195**: p. 877-889.
[37] Qian, C., R. Alrowais, M. Burhan, D. Ybyraiymkul, M.W. Shahzad, L. Yong, and K.C. Ng, *A self-sustainable solar desalination system using direct spray technology.* Energy, 2020: p. 118037.
[38] Zamfirescu, C. and I. Dincer, *How much exergy one can obtain from incident solar radiation?* Journal of Applied Physics, 2009. **105**(4): p. 044911.
[39] Chen, Q., M.K. Ja, Y. Li, and K. Chua, *On the second law analysis of a multi-stage spray-assisted low-temperature desalination system.* Energy conversion and management, 2017. **148**: p. 1306-1316.
[40] Shin, M.-S., H.-S. Kim, D.-S. Jang, S.-N. Lee, Y.-S. Lee, and H.-G. Yoon, *Numerical and experimental study on the design of a stratified thermal storage system.* Applied thermal engineering, 2004. **24**(1): p. 17-27.
[41] Kribus, A., D. Kaftori, G. Mittelman, A. Hirshfeld, Y. Flitsanov, and A. Dayan, *A miniature concentrating photovoltaic and thermal system.* Energy Conversion and Management, 2006. **47**(20): p. 3582-3590.
[42] Andrés-Mañas, J., A. Ruiz-Aguirre, F. Acién, and G. Zaragoza, *Assessment of a pilot system for seawater desalination based on vacuum multi-effect membrane distillation with enhanced heat recovery.* Desalination, 2018. **443**: p. 110-121.
[43] Mittelman, G., A. Kribus, and A. Dayan, *Solar cooling with concentrating photovoltaic/thermal (CPVT) systems.* Energy Conversion and Management, 2007. **48**(9): p. 2481-2490.
[44] Sirkar, K.K. and L. Song, *Pilot-scale studies for direct contact membrane distillation-based desalination process*. 2009: US Department of the Interior, Bureau of Reclamation.
[45] Tavakkoli, S., O.R. Lokare, R.D. Vidic, and V. Khanna, *A techno-economic assessment of membrane distillation for treatment of Marcellus shale produced water.* Desalination, 2017. **416**: p. 24-34.
[46] Ho, W. and K. Sirkar, *Membrane handbook*. 2012: Springer Science & Business Media.
[47] Helal, A., A. El-Nashar, E. Al-Katheeri, and S. Al-Malek, *Optimal design of hybrid RO/MSF desalination plants Part I: Modeling and algorithms.* Desalination, 2003. **154**(1): p. 43-66.
[48] Outlook, A.E., *Energy information administration.* Department of Energy, 2010. **92010**(9): p. 1-15.
[49] Mahmoudi, H., N. Ghaffour, M.F. Goosen, and J. Bundschuh, *Renewable Energy Technologies for Water Desalination*. 2017: CRC Press.
[50] Al-Othman, A., M. Tawalbeh, M.E.H. Assad, T. Alkayyali, and A. Eisa, *Novel multi-stage flash (MSF) desalination plant driven by parabolic trough collectors and a solar pond: A simulation study in UAE.* Desalination, 2018. **443**: p. 237-244.